MELTING HEAT TRANSFER AND THERMAL RADIATION EFFECTS ON MHD TANGENT HYPERBOLIC NANOFLUID FLOW WITH CHEMICAL REACTION AND ACTIVATION ENERGY

by

Salman ZEB[a*], Sapna GUL[a], Kamal SHAH[a,b], Dania SANTINA[b], and Nabil MLAIKI[b]

[a] Department of Mathematics, University of Malakand, Chakdara, Dir (Lower), Pakistan
[b] Department of Mathematics and Sciences, Prince Sultan University, Riyadh, Saudi Arabia

Original scientific paper
https://doi.org/10.2298/TSCI23S1253Z

In this research, we take into account tangent hyperbolic nanofluid flow along a moving stretched surface with thermal radiation, exothermic/endothermic chemical reaction and activation energy effects under melting condition. Governing PDE are transformed to dimensionless non-linear ODE with the add of appropriate similarity variables. The resulting non-linear ODE are solved numerically. The flow parameters influences on the fluid's velocity, temperature, and concentration distributions are investigated. The results revealed that temperature profile is declining while concentration and velocity profiles are increasing for enhancing melting parameter.

Key words: *tangent hyperbolic fluid, melting condition, thermal radiation, activation energy, chemical reaction, magnetohydrodynamics*

Introduction

Fluids that do not adhere to Newton's viscosity law are said to be non-Newtonian fluids. That is, their viscosity or flow behavior changes under stress. These fluids have enormous engineering and industrial applications such as in food, fermentation, chemical, colloidal suspensions, and in biological processes. Constitutive equations representing stress and strain relationship has been suggested in the literature for various non-Newtonian fluids due to non-availability of a single equation for studying and predicting the behavior of these fluids. Tangent hyperbolic fluid is a non-Newtonian fluid predicting shear thinning phenomenon which means that its viscosity decreases with increasing shear stress. Nanofluids are suspensions of nanoparticles in fluids. It has a wide range of industrial and technological utilizations consisting in electronic devices cooling, heat exchangers, nuclear reactors, vehicle cooling, *etc*. Choi and Eastman [1] examined the usage of nanoparticles to improve the thermal conductivity of fluids. As demonstrated by earlier studies [2-6], nanofluids have improved thermophysical properties compared to base fluids, including thermal conductivity, convective heat transfer coefficients, thermal diffusivity, and viscosity. As a result, even at low nanoparticle concentrations, its suspension in base fluids greatly improves their properties.

Nanofluids flow and heat transfer features under various effects with base fluids as non-Newtonian are of great interest in recent years. Prasannakumara *et al*. [7] conducted heat

* Corresponding author, e-mail: salmanzeb@uom.edu.pk

transport study of Sisko nanofluid having non-linear thermal radiation, magnetic field, and chemical reaction effects. Hsiao [8] analysed the radiative flow of Carreau nanomaterials fluid in conjunction with magnetic parameter and activation energy. Gholinia *et al.* [9] elaborated Joule heating and heat generation/absorption on radiative Walters-B nanofluid-flow. Flow of non-Newtonian nanoparticles fluid and heat transport were analysed by Kumar [10] while taking slip factor and chemical reaction into account. Abbas *et al*. [11] conducted theoretical research on a micropolar hybrid nanofluid through a Riga channel having velocity and thermal slip limitations. The heat transfer and flow analysis of chemically radiative tangent hyperbolic nanomaterials fluid having activation energy has been conducted in [12]. Gowda *et al*. [13] discussed mass and heat transport phenomena of chemically reactive MHD flow of second-grade nanofluid while considering activation energy impact. Obalalu *et al*. [14] analyzed Caason fluid-flow with nanoparticles in a porous media along a Riga plate in consideration with chemical reaction, melting condition, magnetic parameter, and activation energy. Casson fluid-flow with nanoparticles along a stretched surface with inclusion of melting condition and magnetic parameter effects examined by Kumar and Uma [15]. Study of Prandtl-Eyring MHD nanoliquid-flow with effects of activation energy, melting condition, and Joule heating has been deliberated by Ullah *et al*. [16].

In this study, we analyze steady incompressible radiative tangent hyperbolic nanofluid flow over a stretching surface in consideration of melting condition, activation energy, chemical reaction, and magnetic field effects. Suitable similarity transformations are used for transforming the governing non-linear PDE of the proposed model into non-dimensional ODE. The resulting non-linear ODE are solved numerically using the built-in command NDSolve in MATHEMATICA software. The concentration, velocity, and temperature profiles of the fluid are sketched and examined in relation to the essential parameters contained in the non-dimensional ODE with boundary conditions.

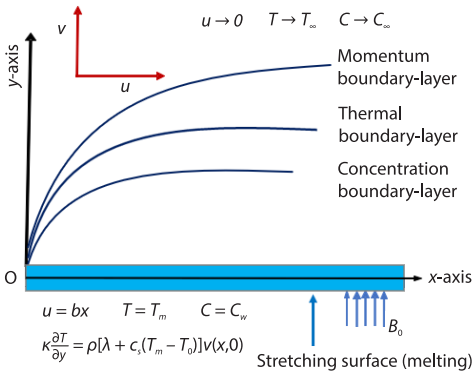

Figure 1. Physical model geometry

Model development

We consider steady laminar flow of incompressible tangent hyperbolic nanofluid in two dimensions. The surface is located at $y = 0$, and the flow occupies the region along $y > 0$ with B_0 as the magnetic field strength normal to the x-axis, and stretching surface velocity is $u_w = bx$, $(b > 0)$. The co-ordinate system and physical geometry sketch is presented in fig. 1. Thermal radiation, exothermic/endothermic chemical reaction and activation energy influences while melting condition at the moving surface has been considered in formulating the governing mathematical model.

The governing equations for the tangent hyperbolic nanofluid-flow in considerations of physical phenomena and effects as described is presented in the following manner [17-19]:

– Continuity equation

$$\frac{\partial u}{\partial x}+\frac{\partial v}{\partial y}=0 \tag{1}$$

– Momentum equation

$$u\frac{\partial u}{\partial x}+v\frac{\partial u}{\partial y}=\nu(1-n)\frac{\partial^2 u}{\partial y^2}+\sqrt{2}\nu n\Gamma\left(\frac{\partial u}{\partial y}\right)\frac{\partial^2 u}{\partial y^2}-\frac{\sigma B_0^2}{\rho}u \tag{2}$$

– Energy equation

$$u\frac{\partial T}{\partial x}+v\frac{\partial T}{\partial y}=\alpha\frac{\partial^2 T}{\partial y^2}+\frac{16\sigma^* T_\infty^3}{3k^*\rho c_p}\frac{\partial^2 T}{\partial y^2}+\tau\left[D_B\left(\frac{\partial C}{\partial y}\frac{\partial T}{\partial y}\right)+\frac{D_T}{D_\infty}\left(\frac{\partial T}{\partial y}\right)^2\right]+$$
$$+\beta_1 k_r^2(C-C_\infty)\left(\frac{T}{T_m}\right)^m\exp\left(\frac{-E_a}{KT}\right) \tag{3}$$

– Concentration equation

$$u\frac{\partial C}{\partial x}+v\frac{\partial C}{\partial y}=D_B\frac{\partial^2 C}{\partial y^2}+\frac{D_T}{T_\infty}\left(\frac{\partial^2 T}{\partial y^2}\right)-k_r^2(C-C_\infty)\left(\frac{T}{T_\infty}\right)^m\exp\left(\frac{-E_a}{KT}\right) \tag{4}$$

with imposed constraints:

$$\text{at } y=0,\ u=bx,\ \kappa\frac{\partial T}{\partial y}=\rho\left[\lambda+c_s(T_m-T_0)\right]v(x,0),\ T=T_m,\ C=C_w$$
$$\text{as } y\to\infty,\ u\to 0,\ T\to T_\infty,\ C\to C_\infty \tag{5}$$

where temperature is denoted by T, C is the nanoparticles volume fraction, u, v – components of velocity field in the x- and y-directions, respectively, E_a – the activation energy, k_r – the rate of reaction, τ – the ratio of heat capacities, κ – the thermal conductivity, K – the Boltzmann constant, β_1 – the endothermic/exothermic reaction coefficient, ν – the kinematic viscosity, n – the power law index, σ – the electrical conductivity, k^* – the absorption coefficient, $-1 < m < 1$ – the fitted rate constant, c_s – the heat capacity of the solid surface, T_m – the melting temperature of the solid surface, λ – the fluid latent heat, T_∞ – the ambient temperature, T_0 – the temperature of the solid surface, C_∞ – the ambient concentration of nanoparticles, $v(x, 0)$ – the velocity component in y-direction, b – the stretching rate, D_T – the thermophoresis diffusion coefficient, c_p – the specific heat at constant pressure, Γ – the time dependent material constant, D_B – the Brownian diffusion coefficient, and ρ – the density of the fluid.

Applying the similarity transformation:

$$\psi=x\sqrt{b\nu}f(\eta),\ \theta(\eta)=\frac{T-T_m}{T_\infty-T_m},\ \eta=\sqrt{\frac{b}{\nu}}y,\ \varphi(\eta)=\frac{C-C_\infty}{C_w-C_\infty} \tag{6}$$

with stream function ψ defined:

$$u=\frac{\partial\psi}{\partial y},\ v=-\frac{\partial\psi}{\partial x} \tag{7}$$

we get the following non-linear ODE from the governing equations of the mathematical model:

$$(1-n)f'''+n\mathrm{We}f'''f''+f''f-[f']^2-M^2f'=0 \tag{8}$$

$$\left(1+\frac{4}{3}R\right)\theta''+\mathrm{Pr}\left(Nb\varphi'\theta'+Nt\theta'^2+f\theta'\right)+\mathrm{Pr}\,\lambda_1\varphi\left(\theta\delta+1\right)^m\exp\left(-\frac{E}{\theta\delta+1}\right)=0 \tag{9}$$

$$\varphi''+\frac{Nt}{Nb}\theta''+\mathrm{Sc}f\varphi'-\mathrm{Sc}\sigma\varphi\left(\theta\delta+1\right)^m\exp\left(-\frac{E}{\theta\delta+1}\right)=0 \tag{10}$$

and corresponding boundary conditions in transformed manner are given:

$$\text{at } \eta=0,\ f'(\eta)=1,\ Me\theta'(\eta)+\mathrm{Pr}\,f(\eta)=0,\ \theta(\eta)=0,\ \varphi(\eta)=1$$
$$\text{as } \eta\to\infty,\ f'(\eta)=0,\ \theta(\eta)=1,\ \varphi(\eta)=0 \tag{11}$$

where power law index is denoted by n,

$$R = \frac{4\sigma^* T_\infty^3}{k^* \kappa}$$

stands for the radiation parameter, Prandtl number is given,

$$\mathrm{Pr} = \frac{\nu}{\alpha}$$

$$Nb = \frac{\tau D_B}{\nu}(C_w - C_\infty)$$

for Brownian motion parameter,

$$\mathrm{We} = \frac{\sqrt{2b}\Gamma u_w}{\sqrt{\nu}}$$

the Weissenberg number,

$$Nt = \frac{\tau D_T}{T_\infty \nu}(T_\infty - T_m)$$

for thermophoretic parameter,

$$\lambda_1 = \frac{\beta_1 (C_w - C_\infty)}{(T_\infty - T_m)}$$

is endothermic/exothermic reaction parameter, magnetic parameter denoted by,

$$M = \sqrt{\frac{\sigma B^2}{\rho b}}$$

$$\mathrm{Sc} = \frac{\nu}{D_B}$$

for Schmidt number,

$$\sigma_1 = \frac{k_r^2}{b}$$

is the reaction rate, temperature difference given,

$$\delta = \frac{(T_\infty - T_m)}{T_m}$$

$$E = \frac{E_a}{K T_m}$$

stands for activation energy, and

$$Me = \frac{c_p (T_\infty - T_m)}{\lambda + c_s (T_m - T_0)}$$

is the melting parameter, and prime denoting differentiation with respect to η.

Numerical results and discussion

The non-linear ODE (8)-(10) along with constraints (11) are solved numerically using built-in command NDSolve in MATHEMATICA software. Investigation to study the influence of the parameters involved in the transformed equations and boundary conditions is performed.

The velocity profile against magnetic parameter, M, plotted in fig. 2(a) demonstrates declining behavior for enhanced magnetic parameter values which is due to presence of the opposing Lorentz force reducing fluid-flow. Temperature profile is decreasing for rise in magnetic parameter which is presented in fig. 2(b). The concentration field observing an increasing behavior for higher magnetic parameter values which is seen in fig. 2(c). Enhancing the Weissenberg number, extends the relaxation period, which causes higher flow resistance and reduces fluid velocity as presented in fig. 3(a). Figures 3(b) and 3(c) discloses that temperature of the fluid declines while concentration profile enhances as the Weissenberg number increases. The effects of melting parameter, Me, is depicted in figs. 4(a)-4(c) which shows that velocity and concentration profile exhibiting increasing behavior while temperature field is declining for an enhancement in melting parameter. The declining trend in the temperature field is attributed to the higher temperature difference between the ambient and melting surface as a result of increase in the melting parameter. In figs. 5(a)-5(c), we see that velocity and temperature profiles showing declining trend whereas an increasing trend of the concentration field is depicted for enhancing power law index parameter n. Figure 6(a) illustrated that when radiation parameter,

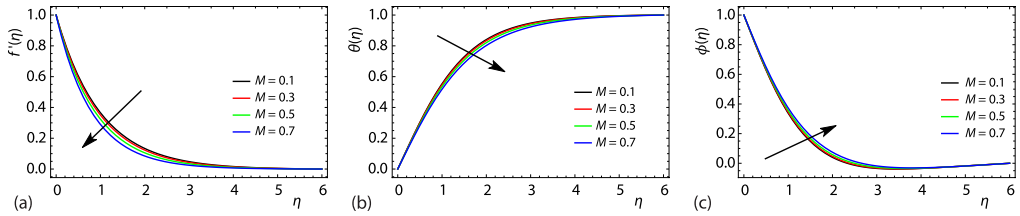

Figure 2. Variations in $f'(\eta)$, $\theta(\eta)$, and $\varphi(\eta)$ via M; (a) $f'(\eta)$ against M, (b) $\theta(\eta)$ via M, and (c) $\varphi(\eta)$ via M

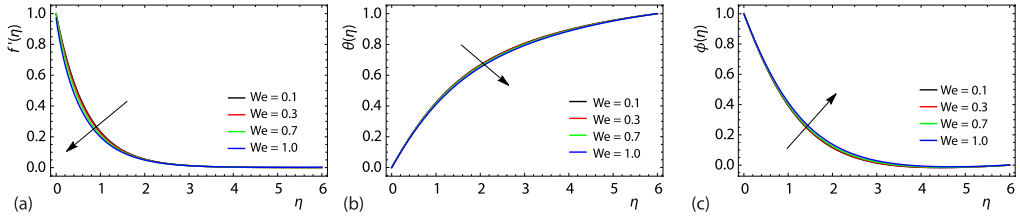

Figure 3. The We influence on velocity, temperature, and concentration; (a) $f'(\eta)$ against We, (b) $\theta(\eta)$ *vs.* We, and (c) $\varphi(\eta)$ *vs.* We

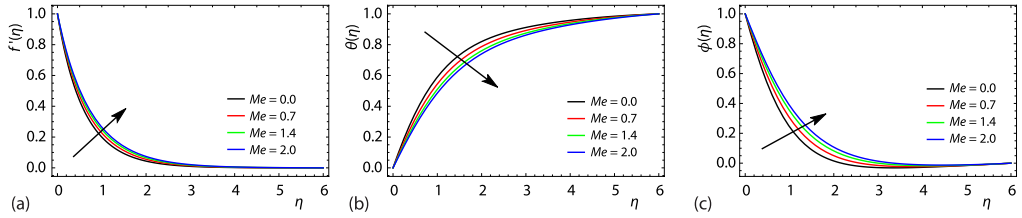

Figure 4. Melting parameter influence on $f'(\eta)$, $\theta(\eta)$, and $\varphi(\eta)$; (a) $f'(\eta)$ against Me, (b) $\theta(\eta)$ *vs.* Me, and (c) $\varphi(\eta)$ *vs.* Me

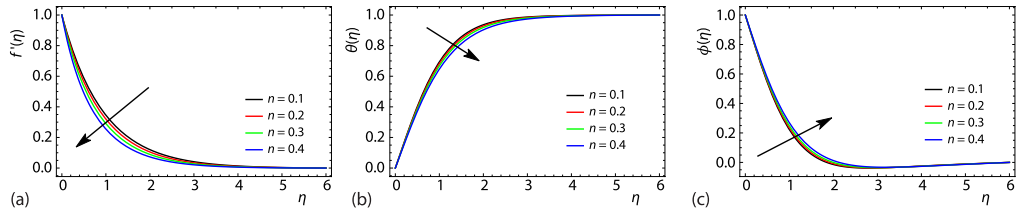

Figure 5. Variations in velocity, temperature, and concentration against *n;* (a) $f'(\eta)$ against *n*, (b) $\theta(\eta)$ *vs.* *n*, and (c) $\varphi(\eta)$ *vs.* *n*

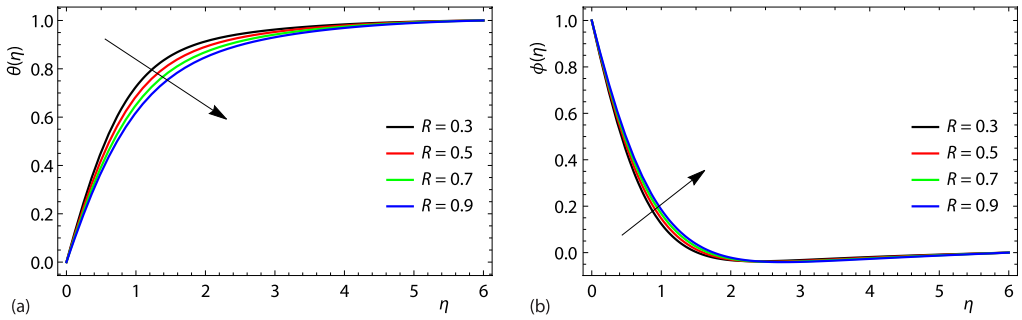

Figure 6. Radiation parameter effects on temperature and concentration profiles; (a) $\theta(\eta)$ *vs.* *R* and (b) $\varphi(\eta)$ *vs.* *R*

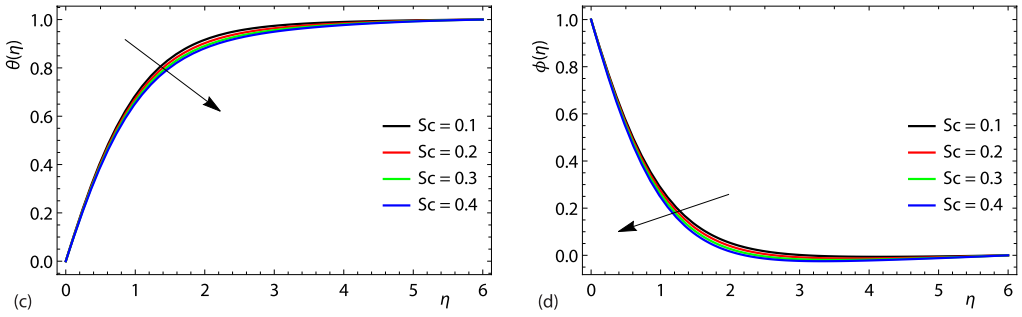

Figure 7. Behavior of $\theta(\eta)$ and $\varphi(\eta)$ via Sc; (a) $\theta(\eta)$ *vs.* Sc and (b) $\varphi(\eta)$ *vs.* Sc

R, is increased, the temperature profile declines. The increasing behavior of the concentration profile can be seen against rising thermal radiation parameter in fig. 6(b). Temperature shows a decreasing trends for enhancing Schmidt number as depicted in fig. 7(a). The rising Schmidt number, reduces mass diffusivity which implies concentration profile is declining as predicted in fig. 7(b). Enhancing reaction rate, σ_1, increasing temperature field as illustrated in fig. 8(a). In fig. 8(b), the impact of the rising reaction rate values depicts the declining behavior of concentration distribution. Both temperature and concentration distributions are decreasing when thermophoretic parameter, *Nt*, is enhanced as presented in figs. 9(a) and 9(b). Figure 10(a) illustrates that temperature field is a decreasing function against rising Brownian motion parameter, *Nb*. The concentration profile is increasing when *Nb* values are enhanced as seen in fig. 10(b). In fig. 11(a), enhancing λ_1 values provides extra heat to the nanoparticles due to exothermic reaction and hence the temperature profile rises. The concentration profile decreases when λ_1 values are enhanced as observed in fig. 11(b). Increasing behavior for temperature field in fig. 12(a) and a decreasing trend for concentration profile in fig. 12(b) are depicted for enhancing temperature difference parameter δ.

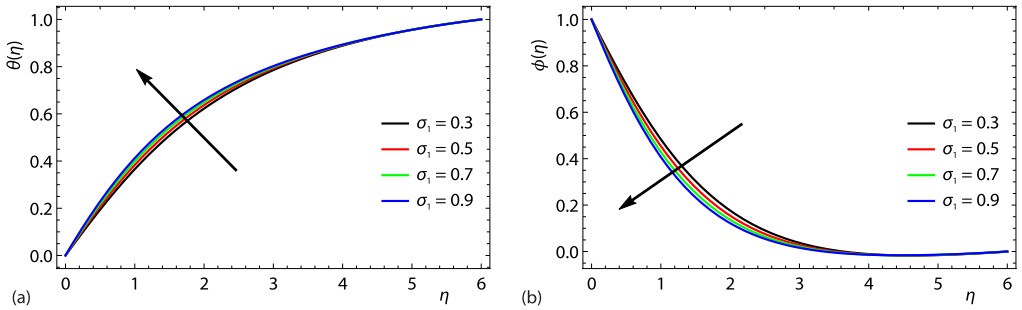

Figure 8. Reaction rate influence on temperature and concentration fields; (a) $\theta(\eta)$ *vs.* σ_1 and (b) $\varphi(\eta)$ *vs.* σ_1

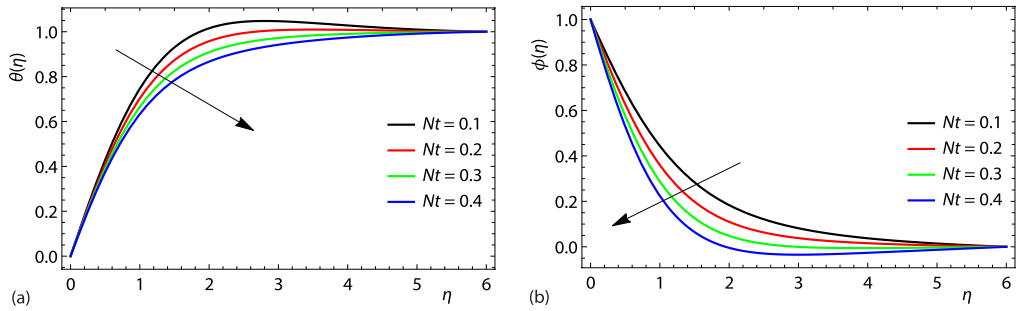

Figure 9. Thermophoretic parameter influence on $\theta(\eta)$ and $\varphi(\eta)$; (a) $\theta(\eta)$ *vs.* *Nt* and (b) $\varphi(\eta)$ *vs.* *Nt*

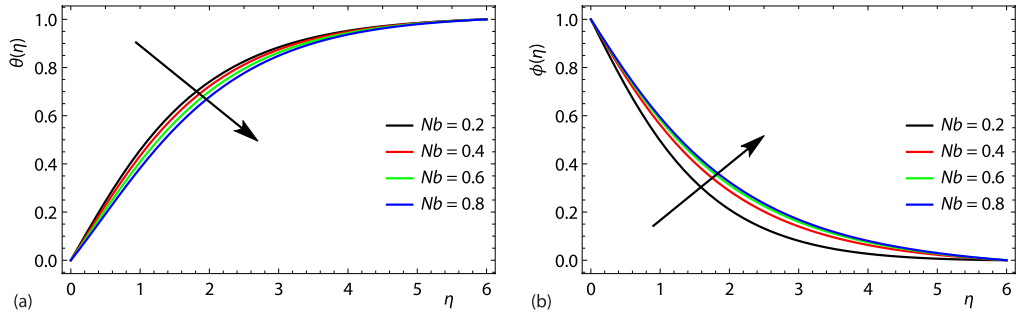

Figure 10. Brownian parameter effects on temperature and concentration profiles; (a) $\theta(\eta)$ *vs.* *Nb* and (b) $\varphi(\eta)$ *vs.* *Nb*

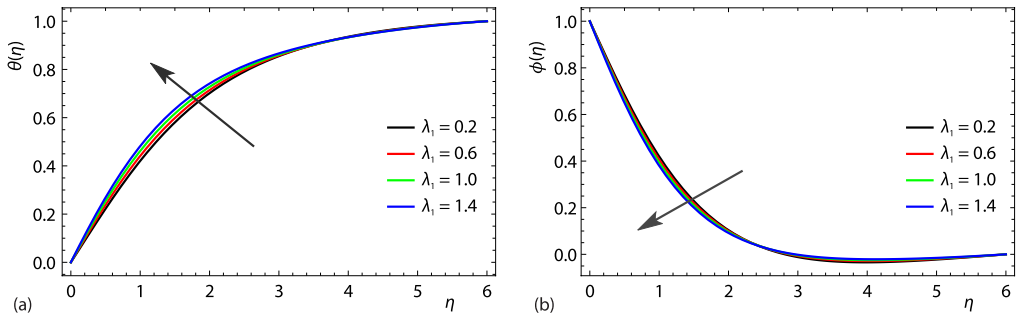

Figure 11. Influence of endothermic/exothermic reaction parameter on temperature and concentration profiles; (a) $\theta(\eta)$ *vs.* λ_1 and (b) $\varphi(\eta)$ *vs.* λ_1

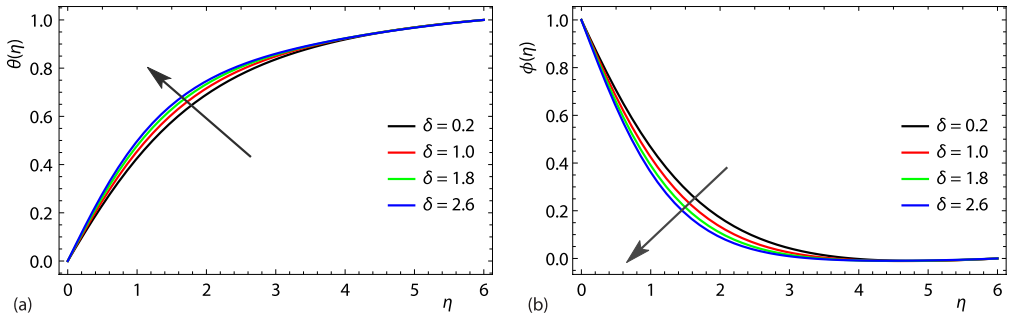

Figure 12. Temperature difference parameter effects on temperature and concentration profiles; (a) $\theta(\eta)$ *vs.* δ and (b) $\phi(\eta)$ *vs.* δ

Conclusion

We considered steady incompressible radiative MHD tangent hyperbolic nanofluid laminar flow model with effects of melting phenomena, exothermic/endothermic chemical reaction, and activation energy. The numerical results of the transformed ODE are computed and graphical representations are provided. The results reported showed declining trends for velocity and temperature while concentration profile is increasing for enhancing magnetic parameter, Weissenberg number, and power law index values. Temperature distribution diminishes with enhancing values of *Me*, *R*, *Nt*, *Nb*, and Sc, whereas a reverse trend is visualized for augmentation in σ_1, δ, and λ_1. Moreover, concentration profile declining in respect of thermophoretic parameter, endothermic/exothermic reaction parameter, temperature difference parameter, Schmidt parameter, and reaction rate while increase in the concentration profile is depicted when *Me*, *Nb*, and *R* parameters values are increased.

Acknowledgment

The authors K. Shah, D. Santina and N. Mlaiki would like to thank Prince Sultan University for paying the publication fees for this work through TAS LAB.

References

[1] Choi, S. U. S., Eastman, J. A., Enhancing Thermal Conductivity of Fluids with Nanoparticles, (No. ANL/MSD/CP-84938; CONF-951135-29), Argonne National Lab. (ANL), Argonne, Ill., USA, 1995
[2] Choi, S. U. S., Nanofluids: From Vision Reality through Research, *Journal Heat Transfer*, 131 (2009), 3, 033106
[3] Yu, W., *et al*., Review and Comparison of Nanofluid Thermal Conductivity and Heat Transfer Enhancements, *Heat Transf. Eng*., *29* (2008), 5, pp. 432-460
[4] Tyler, T., *et al*., Thermal Transport Properties of Diamond-Based Nanofluids and Nanocomposites, *Diam. Relat. Mater*., *15* (2006), 11-12, pp. 2078-2081
[5] Das, S. K., Heat Transfer in Nanofluids – A Review, *Heat Transf. Eng*., *27* (2006), 10, pp. 3-19
[6] Liu, M. S., *et al*, Enhancement of Thermal Conductivity with Carbon Nanotube for Nanofluids, *Int. Commun. Heat Mass Transf*., *32* (2005), 9, pp. 1202-1210
[7] Prasannakumara, B. C., *et al*., The MHD Flow and Non-Linear Radiative Heat Transfer of Sisko Nanofluid over a Non-Linear Stretching Sheet, *Inform. Med. Unlocked*., *9* (2017), C, pp. 123-132
[8] Hsiao, K. L., To Promote Radiation Electrical MHD Activation Energy Thermal Extrusion Manufacturing System Efficiency by Using Carreau-Nanofluid with Parameters Control Method, *Energy, 130* (2017), July, pp. 486-499
[9] Gholinia, M., *et al*., A Numerical Investigation of Free Convection MHD Flow of Walters-B Nanofluid over an Inclined Stretching Sheet under the Impact of Joule Heating, *Therm. Sci. Eng. Prog*., *11* (2019), June, pp. 272-282

[10] Kumar, K. G., Exploration of Flow and Heat Transfer of non-Newtonian Nanofluid over a Stretching Sheet by Considering Slip Factor, *Int. J. Numer. Method Heat Fluid-Flow*, *30* (2019), 4, pp. 1991-2001
[11] Abbas, N., *et al*., Theoretical Study of Micropolar Hybrid Nanofluid over Riga Channel with Slip Conditions, *Phys. A: Stat. Mech. Appl*., 551 (2020), 124083
[12] Kumar, K. G., *et al*., Significance of Arrhenius Activation Energy in Flow and Heat Transfer of Tangent Hyperbolic Fluid with Zero Mass Flux Condition, *Microsyst. Technol*., *26* (2020), 8, pp. 2517-2526
[13] Gowda, R. J. P., *et al*., Impact of Binary Chemical Reaction and Activation Energy on Heat and Mass Transfer of Marangoni Driven Boundary-Layer Flow of a Non-Newtonian Nanofluid, *Processes*, *9* (2021), 4, 702
[14] Obalalu, A. M., *et al.*, Effect of Melting Heat Transfer on Electromagnetohydrodynamic Non-Newtonian Nanofluid-Flow over a Riga Plate with Chemical Reaction and Arrhenius Activation Energy, *Eur. Phys. J. Plus*, *136* (2021), 8, pp. 1-16
[15] Kumar, T. P., Uma, M. S., The MHD Casson Nanofluid-Flow over a Stretching Surface with Melting Heat Transfer Condition, *Heat Transfer*, *51* (2022), 8, pp. 7328-7347
[16] Ullah, I., *et al*., Theoretical Analysis of Activation Energy Effect on Prandtl-Eyring Nanoliquid-Flow Subject to Melting Condition, *Journal Non-Equil. Thermody*., *47* (2022), 1, pp. 1-12
[17] Maleque, K. A., Effects of Binary Chemical Reaction and Activation Energy on MHD Boundary-Layer Heat and Mass Transfer Flow with Viscous Dissipation and Heat Generation/Absorption, *Int. Sch. Res. Notices*, *2013* (2013), ID284637
[18] Kumar, K. G., *et al*., An Unsteady Squeezed Flow of a Tangent Hyperbolic Fluid over a Sensor Surface in the Presence of Variable Thermal Conductivity, *Results Phys*., *7* (2017), pp. 3031-3036
[19] Dhlamini, M., *et al*., Activation Energy and Binary Chemical Reaction Effects in Mixed Convective Nanofluid-Flow with Convective Boundary Conditions, *Journal Comput. Des. Eng*., *6* (2019), 2, pp. 149-158

Paper submitted: April 1, 2022
Paper revised: April 4, 2022
Paper accepted: April 14, 2022